

d-SEAMS: Deferred Structural Elucidation Analysis for Molecular Simulations

Rohit Goswami,[‡] Amrita Goswami,[‡] and Jayant K. Singh*



Cite This: *J. Chem. Inf. Model.* 2020, 60, 2169–2177



Read Online

ACCESS |



Metrics & More

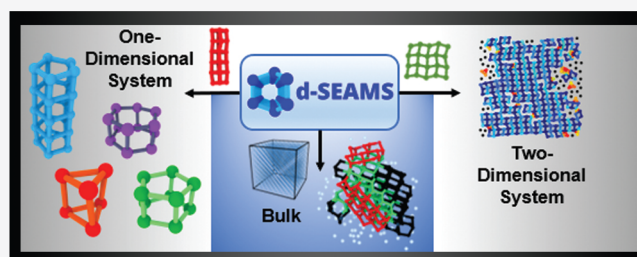


Article Recommendations



Supporting Information

ABSTRACT: Structural analyses are an integral part of computational research on nucleation and supercooled water, whose accuracy and efficiency can impact the validity and feasibility of such studies. The underlying molecular mechanisms of these often elusive and computationally expensive processes can be inferred from the evolution of ice-like structures, determined using appropriate structural analysis techniques. We present d-SEAMS, a free and open-source postprocessing engine for the analysis of molecular dynamics trajectories, which is specifically able to qualitatively classify ice structures in both strong-confinement and bulk systems. For the first time, recent algorithms for confined ice structure determination have been implemented, along with topological network criteria for bulk ice structure determination. We also propose and validate a new order parameter for identifying the building blocks of quasi-one-dimensional ice. Recognizing the need for customization in structural analysis, d-SEAMS has a unique code architecture built with nix and employing a YAML-Lua scripting pipeline. The software has been designed to be user-friendly and extensible. The engine outputs are compatible with popular graphics software suites, allowing for immediate visual insights into the systems studied. We demonstrate the features of d-SEAMS by using it to analyze nucleation in the bulk regime and for quasi-one- and quasi-two-dimensional systems. Structural time evolution and quantitative metrics are determined for heterogeneous ice nucleation on a silver-exposed β -AgI surface, homogeneous ice nucleation, flat monolayer square ice formation, and freezing of an ice nanotube.



INTRODUCTION

The increases in power and efficiency of high-performance computing resources have enabled researchers to directly observe nucleation events in molecular dynamics simulations. Concomitantly, the determination of ice-like structures from simulations is essential for the interpretation of nucleation events, since trajectories provide positional data on particles and do not explicitly track crystal structures and defects.¹ Nucleation of soft matter is further complicated by the emergence of competing ice polymorphs^{2,3} with small free energy differences.⁴ The ice-like structures formed are also continually distorted by thermal fluctuations, which locally disrupt the long-range order. These issues can make automated and accurate structural determination intractable, especially for weakly crystalline regions.⁵ Surface interactions and confinement can strongly influence nucleation behavior,^{6–8} adding to the complexity of the structure determination problem.

Water is a deceptively simple molecule, exhibiting rich and complex phase behavior in bulk and confinement.^{9–19} At least 17 bulk ice polymorphs have been observed experimentally.^{20,21} Water confined within nanometer length scales exhibits even more diversity, forming ordered hydrogen-bonding networks (HBNs) of ice nanotubes, monolayers, bilayers, and trilayers.^{17,22–28} Structural determination of the several possible polymorphs of water, in bulk and in

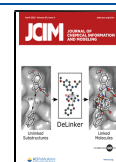
confinement, is of crucial importance in the qualitative and quantitative analysis of simulation data. Analysis of the evolution of ordered structures during a nucleation event is desirable since it can reveal details of the underlying molecular mechanism and provide important physical insights into the system.

In this work, we present d-SEAMS, a cohesive postprocessing structural analysis engine that is capable of coherently classifying water structures under strong confinement and in bulk systems, from quasi-one and two-dimensional confinement to bulk ice polymorphs. Confined ice polymorphs are often identified “by eye” wherein the HBN is manually inspected.^{17,19,26} In particular, d-SEAMS automates the process of structural analysis and qualitative metric calculation, eliminating the need for visual inspection.

Conflicting package clashes due to transitive or indirect dependencies is a recurring problem in software development

Received: January 14, 2020

Published: March 20, 2020



and use.²⁹ Resolving such issues can often be nontrivial, relying on removal of unnecessary dependencies, system updates (for most Linux clusters), and other manual strategies that may be ineffective for a complex dependency tree. These manual strategies are increasingly difficult to carry out on restricted-access machines with high up-times, which are common to high-performance computing (HPC) clusters used for such computationally demanding simulations.

d-SEAMS circumvents the problem of “dependency hell” by using `nix`³⁰ to generate reproducible dependency build-graphs.³¹ Users can run d-SEAMS using the exact build environment of the developers and vice versa, bypassing installation and use issues on various systems and HPC clusters, ensuring reproducible results.

The parameters of structural analysis techniques are often tweaked to suit the specific requirements of the desired study.^{32,33} d-SEAMS has been designed to permit extensions to the code and the implementation of custom workflows. The engine simultaneously incorporates user-friendly interface functions without compromising on functionality. Key features implemented include a primitive ring analysis algorithm,³⁴ topological network criteria for bulk³⁵ and confined systems,³⁶ and new qualitative order parameters. Popular analysis techniques, including bond orientational parameters^{32,37} and related criteria,^{38,39} have also been implemented. Outputs are produced in formats compatible with popular visualization software suites, including OVITO⁴⁰ and VMD.⁴¹ We describe how d-SEAMS has been used to analyze and characterize ice nucleation on an ice-promoting AgI surface, homogeneous bulk nucleation, the formation of monolayer ice, and the freezing of a quasi-one-dimensional ice nanotube (INT).

CODE ARCHITECTURE

Nix Expressions for Reproducible Builds. Computational software implemented in declarative package management systems suffers from design concerns for the end users and the developers. The developers have the onus to package their software as per the many imperative systems (Ubuntu and apt, RedHat and yum, ArchLinux and pacman). Additionally, the users must ensure that the interrelated dependencies match perfectly. In essence, the issue is that the packages and versions at the time of build are not guaranteed automatically at the user's end, even if the software is packaged appropriately for the operating system. This issue stems from the fact that the configuration after installation is the result of a series of stateful transformations that cannot be reproduced.⁴² We have opted to use `nix` to orchestrate version dependencies and abstract such cross-compatibility build nuances. The underlying build system leverages CMake. More details on the design rationale are provided in the [Supporting Information](#).

Pipeline of Workflows. Figure 1 visually depicts the logical pipeline of typical workflows in d-SEAMS. An input system can either be a bulk system, a quasi-one-dimensional system, or a quasi-two-dimensional system. The criteria and analysis algorithms tend to differ across scales as well. Thus, we have separated the mutually exclusive workflows for bulk, quasi-one-dimensional, and quasi-two-dimensional systems, with separate modular code blocks for each type of system. The general software pipeline is organized as follows:

- The user chooses whether the system is a bulk, quasi-one-dimensional, or quasi-two-dimensional system by setting the appropriate values in the YAML input file.

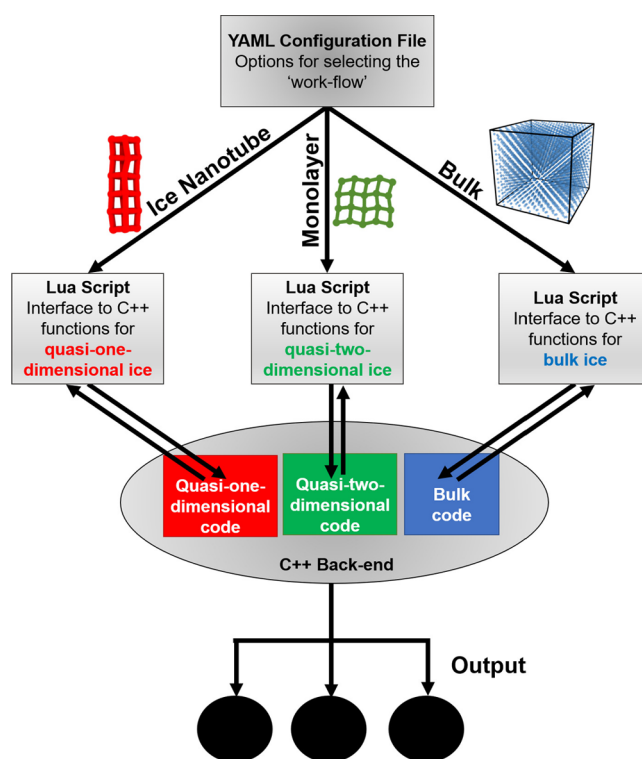


Figure 1. Code pipeline of d-SEAMS. The YAML script file provides options to choose the type of system (bulk, quasi-one-dimensional, or quasi-two-dimensional monolayer) and the corresponding workflow. The Lua interface functions interact with the C++ functions for each workflow, and functions of other workflows are not exposed to the user.

- The Lua script calls the functions to read in and analyze the data and output the desired results.
- Simulation data are read from LAMMPS trajectory files. The XYZ file format is also currently supported. Other file formats may be converted into an ASCII LAMMPS trajectory format.⁴³
- Options for controlling the output results can be specified in the Lua file input. More details on the types of outputs generated by d-SEAMS and how to visualize them are provided in the [Supporting Information](#).
- Output directories are created automatically according to the chosen workflow.

Structural Identification Features. We are able to apply arbitrary transformations on the particle collections in an efficient and idiomatic manner. Currently we have implemented the following structural schemes based on this flexible and extensible framework:

- The bond orientational parameters^{32,37} and CHILL³⁸ and CHILL+³⁹ parameters have been implemented. Clustering of ice-like molecules⁴⁴ based on these parameters can be optionally carried out by the user. The largest ice cluster so obtained can also be recentered for ease of visualization.
- Topological network criteria for bulk ice determination³⁵ have been implemented. d-SEAMS is able to identify and write out detailed information about double-diamond cages (DDCs), hexagonal cages (HCs), and mixed rings for every frame. Additionally,

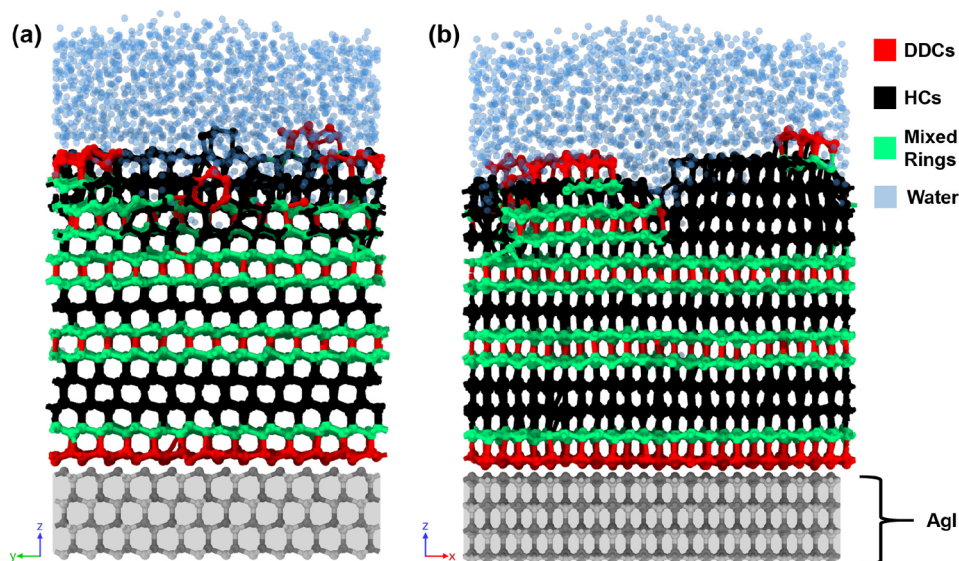


Figure 2. (a) YZ-plane and (b) XZ-plane views of layered hexagonal ice (Ih) and cubic ice (Ic) after 200 ns. DDCs, HCs, and mixed rings are colored in red, black, and green, respectively. The silver and iodine atoms are shown in dark-gray and gray, respectively, with the AgI sheet highlighted in light gray.

the numbers of basal and prismatic rings are also computed.

- Primitive rings are identified. First, all possible rings are found using an exhaustive backtracking algorithm, following which non-shortest-path rings are removed.³⁴ Ring networks with only hydrogen-bonded connections can be optionally determined.
- Confined quasi-two-dimensional ice is classified by topological and graph-theoretic approaches to the hydrogen-bonded ice-like particles.
- Quasi-one-dimensional ice nanotube (INT) and quasi-two-dimensional monolayer ice are classified via topological network criteria.³⁶ The building blocks of n -gonal prismatic ice are explicitly and unequivocally identified.
- d-SEAMS is capable of calculating geometric order parameters for describing the phase transitions in confined ice.

■ APPLICATIONS

Using d-SEAMS, structural and qualitative information as a time series can be directly obtained. This makes it possible to study a variety of diverse nucleating systems. The mechanism of nucleation growth can also be inferred from an ensemble of trajectories by analyzing the qualitative metrics supported by d-SEAMS. We have used the outputs of d-SEAMS, visualized in OVITO,⁴⁰ to create the visuals in this work.

Bulk Systems. Heterogenous Nucleation on an Ice-Promoting Surface. Silver iodide is an effective ice nucleating agent, whose lattice closely resembles that of bulk ice.⁴⁵ The smooth Ag-exposed β -AgI surface has been known to promote layer-by-layer growth of hexagonal ice (Ih) and cubic ice (Ic) in simulations.⁴⁶ Using d-SEAMS, we probe the underlying mechanism of the ice nucleation growth and behavior. Ten independent simulations of 5120 TIP4P/Ice⁴⁷ molecules on a free-standing AgI surface were run up to ~ 200 ns at 240 K. The simulation setup is similar to that of previous work in the literature.⁴⁸

Here we employ a topological network criterion³⁵ for identifying the building blocks of Ih and Ic, namely, hexagonal cages (HCs) and double-diamond cages (DDCs), respectively. Rings that belong to both HCs and DDCs are classified as mixed rings.

Figure 2 depicts layers of HCs and DDCs growing from the AgI surface after 200 ns of simulation time. The close lattice match between the AgI surface and the ice phases is clearly visible. However, the CHILL algorithm³⁸ identifies the first layer of molecules close to the surface as liquid. It was noted in previous studies that although the CHILL algorithm does not identify the first layer of water molecules as ice, these molecules actually form part of the initial ice layer.^{46,49} The topological network criterion used here correctly classifies these water molecules as constituents of HCs or DDCs.

The Ag-exposed β -AgI surface supports the attachment of the basal planes of HCs and DDCs. Figure 3 shows how layers grow through the attachment of HCs and DDCs.

The peripheral rings of DDCs can support the attachment of both HCs and DDCs. However, the prismatic planes of an HC (highlighted in blue, green, and mauve in Figure 3b) can only support the anchoring of HCs. Since the HCs grow upward from the AgI surface through the basal plane (highlighted in yellow in Figure 3a), only HCs can grow from the prismatic planes of pre-existing HCs in each layer. We surmise that the layerwise growth of HCs in the lateral dimensions is a result of this growth behavior. This is in keeping with the stacking effects observed in the literature.⁴⁸

The effect of the surface is the most significant within the first two layers of cages. In all of the independent trajectories, a single layer of either HCs or DDCs is formed first, upon which a second layer of DDCs grows. The two possible outcomes of the stacking of cages, observed in independent simulations, are depicted visually in Figure 4. Figure 4a shows an overhead view of the stacking arrangement when the first layer and second layer are HCs and DDCs, respectively. Figure 4b shows the other stacking arrangement observed, wherein the first and second layers are exclusively composed of DDCs. Both types of arrangements seem equally likely on the basis of the roughly

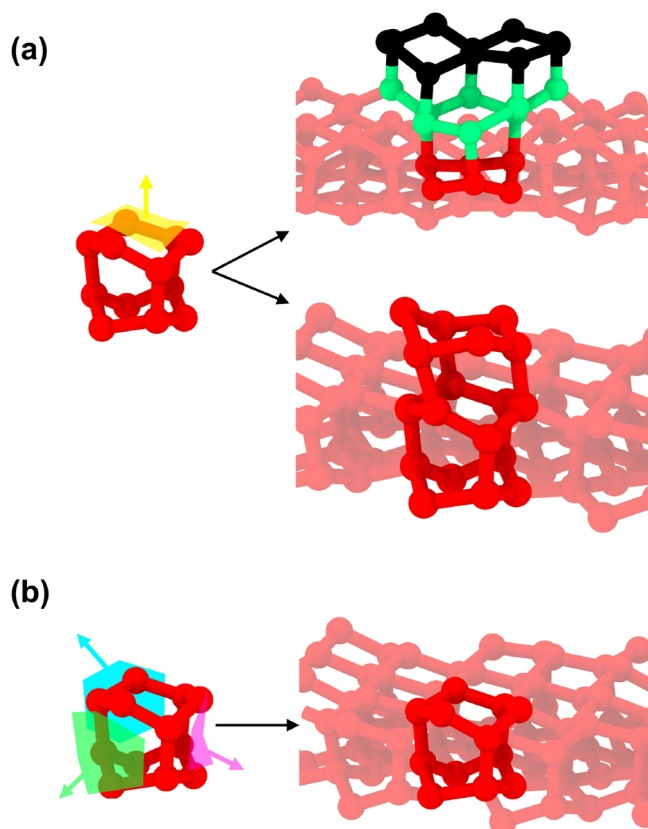


Figure 3. (a) Attachment of cages on the upper basal face of an HC. The basal face is highlighted in yellow. Basal faces of an HC can support the growth of both DDCs (black) and HCs (red). (b) Attachment of HCs on the three prismatic faces, shaded in blue, green, and mauve, of an HC. The prismatic faces of an HC cannot support the growth of DDCs. The color scheme is the same as in Figure 2.

equal proportions of stacking observed in all of the independent simulations performed. Regardless of the composition of the first two layers, alternating layers of varying widths of HCs and DDCs are formed in all of the simulations. Interestingly, although HCs sometimes grow on the first layer, by the end of the simulations, the second layer is exclusively composed of DDCs.

We track the growth of the first two layers with time for a particular trajectory, whose stacking at the end of 200 ns is shown in Figure 4a.

Figure 5 shows the growth of the first two layers of cages within the first 100 ns of simulation time. After ~ 60 ns, the second layer is partially composed of HCs and DDCs (Figure 5b). The HC portion is not anchored to the DDC part of the second layer, since DDCs cannot grow on the exposed lateral prismatic faces of the HCs. We note that eventually, by the time that the second layer of cages becomes continuous, HCs in the second layer disappear and are completely replaced by DDCs. In fact, the eventual layering of HCs and DDCs in the first two layers from the AgI surface is also observed on void-defect-incorporated Ag-exposed β -AgI surfaces.⁴⁸

Homogenous Nucleation: Growth of the Largest Ice Cluster. Here we analyzed a trajectory that exhibits a successful homogeneous nucleation event in the bulk phase. Independent simulations of 4096 particles, modeled using the monatomic water (mW) water model,⁵⁰ were equilibrated at 300 K and quenched to 208 K. Simulations were subsequently run at constant temperature and pressure in the *NPT* ensemble at 1 atm and 208 K for up to 1 μ s. Figure 6 shows the structural features and growth of the largest ice cluster. In our ensemble of trajectories, we observe that the largest ice crystallites that survive and grow to the postcritical size are rich in DDCs (shown in black in Figure 6). We find that even in postcritical crystallites, the core of the crystallites remains rich in DDCs. These findings match those gleaned from extensive forward-flux sampling simulations of both mW water and TIP4P/Ice.³⁵

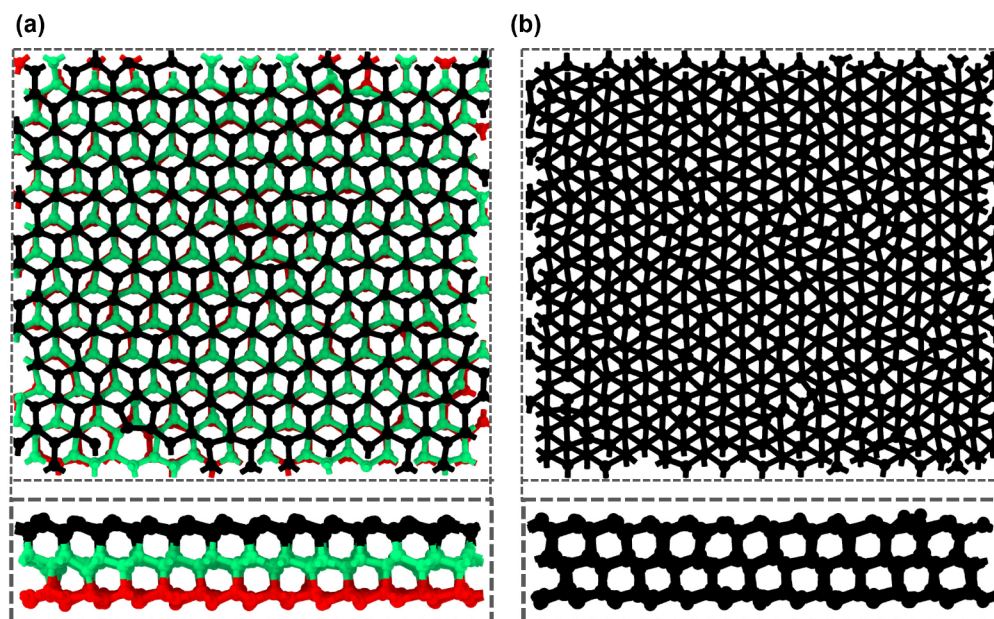


Figure 4. Overhead and side views showing the stacking arrangements of the first two layers of cages on the AgI surface, when more than half the water has been converted to ice, after more than ~ 150 ns of simulation time. (a) The first layer is a layer of HCs. The complete second layer is a layer of DDCs in all cases observed. Mixed rings are sandwiched between the first layer of HCs and the second layer of DDCs. (b) The first and second layers are DDCs. The color scheme is the same as in the preceding figures.

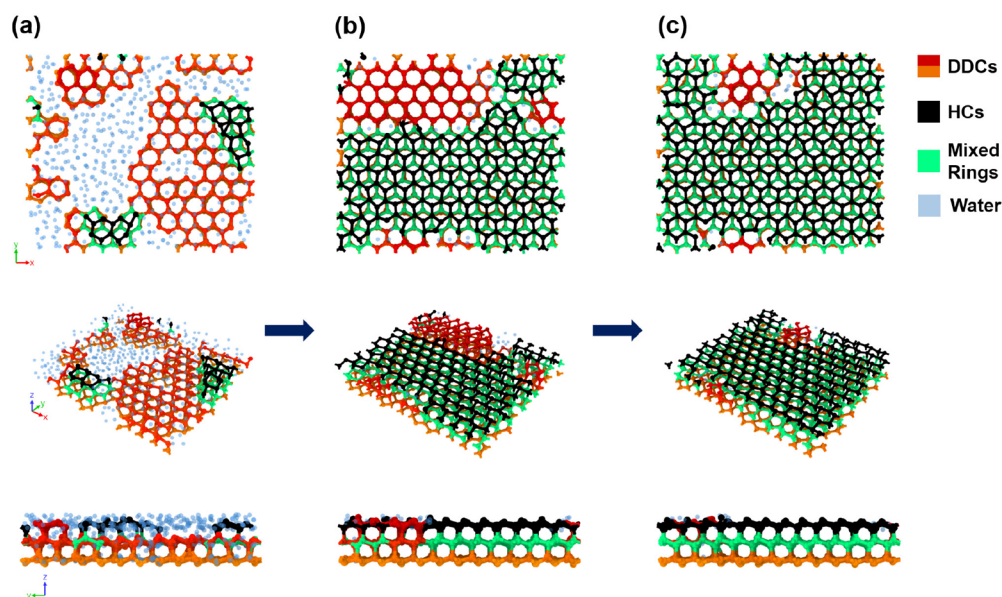


Figure 5. Formation of layers of HCs and DDCs within the first 100 ns of simulation time. (a) After ~ 14 ns, the first layer has not completely formed. (b) After ~ 60 ns, part of the second layer is composed of HCs, and a separate portion of the second layer is composed of DDCs. The part of the second layer made up of HCs is distinguishable in the top view because of the AA stacking order of HCs on the first layer of HCs. (c) After ~ 100 ns, the second layer is almost entirely composed of DDCs. The color scheme is shown in the legend. DDCs are colored in shades of yellow to vermilion according to the distance from the AgI surface.

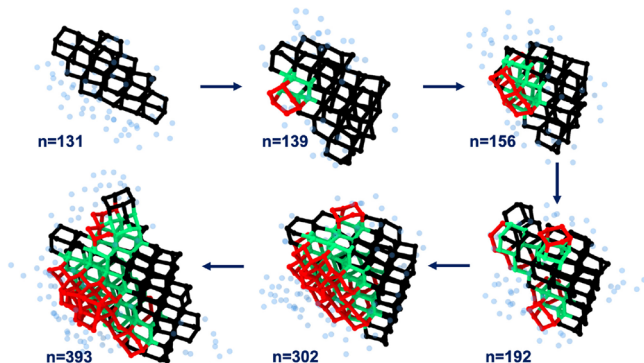


Figure 6. Evolution of an ice crystallite of mW water at 208 GPa in the *NPT* ensemble. DDCs are shown in black, HCs in red, and mixed rings belonging to both DDCs and HCs in green. The number of particles in the largest cluster, n , is shown for every snapshot of the trajectory. Water molecules that do not participate in the cages are shown in transparent blue.

The growth of the largest crystallite with time, showing fluctuations in the cluster size with time, is depicted in a [movie in the Supporting Information](#).

Quasi-Two-Dimensional Systems. We also analyze flat monolayer square ice (fMSI) using d-SEAMS. fMSI has been observed in simulations when water subjected to a lateral pressure of 1 GPa is sandwiched between rigid graphene sheets separated by a slit width of 6 Å.^{26,51} d-SEAMS is capable of calculating the coverage area metric,³⁶ an area-based order parameter, at every time step of a trajectory. We demonstrate the efficacy of the coverage area metric in describing phase transitions during the cooling of a quasi-two-dimensional monolayer from 320 K to 310 K over 1 ns. The visuals produced were generated from the output of d-SEAMS. [Figure 7](#) shows snapshots of monolayer water through various stages of cooling, exhibiting a gradual increase in the proportion of the four-membered rings. At 320 K, the coverage area of the

four-membered rings is $\sim 70\%$, which indicates that the monolayer is predominantly fMSI. This phase change is depicted in a [movie in the Supporting Information](#).

d-SEAMS is also capable of calculating the in-plane radial distribution function. The solidlike ordered nature of the ice formed at 310 K is typified by the shape of the two-dimensional oxygen–oxygen radial distribution function in [Figure 8](#). $g_{OO}(r)$ has the highest peak at 2.775 ± 0.05 Å, followed by a shoulder peak and a third smaller peak; the same features have been observed previously for fMSI. The frames were obtained from an equilibrated 1 ns run at a constant temperature of 310 K and lateral pressure of 1 GPa.

[Table 1](#) summarizes the ring statistics and coverage area metric values determined by d-SEAMS for the fMSI structure formed at 310 K. The coverage area metric is a more intuitive and more stable metric than the number of rings, as is evident from the data. The number of rings is more sensitive to small thermal fluctuations that are not relevant to the overall classification scheme.

Quasi-One-Dimensional Systems. [Figure 9](#) shows perspective views of ice nanotubes (INTs) for water constrained within (13,0) and (11,0) zigzag smooth featureless single-walled nanotubes (SWNTs). For the SWNTs, $R = 13$ and $R = 11$ correspond to diameters of 10.1 and 8.6 Å, respectively.

At an axial pressure of $P_{zz} = 0.1$ MPa, primarily hexagonal prism blocks are formed within the INT in [Figure 9a](#). A small proportion of the ice nanoribbon is composed of pentagonal prism blocks, while the rest are deformed prism blocks classified as an “unclassified” phase. The unclassified phase may include deformed prisms, the liquid phase, and hollow helices, which are not explicitly differentiated using the prism classification scheme. In this particular case, the hollow nature of the nanoribbon and the interspersed positions of the unclassified phase between prism blocks indicate that the unclassified phase is composed of deformed prisms.

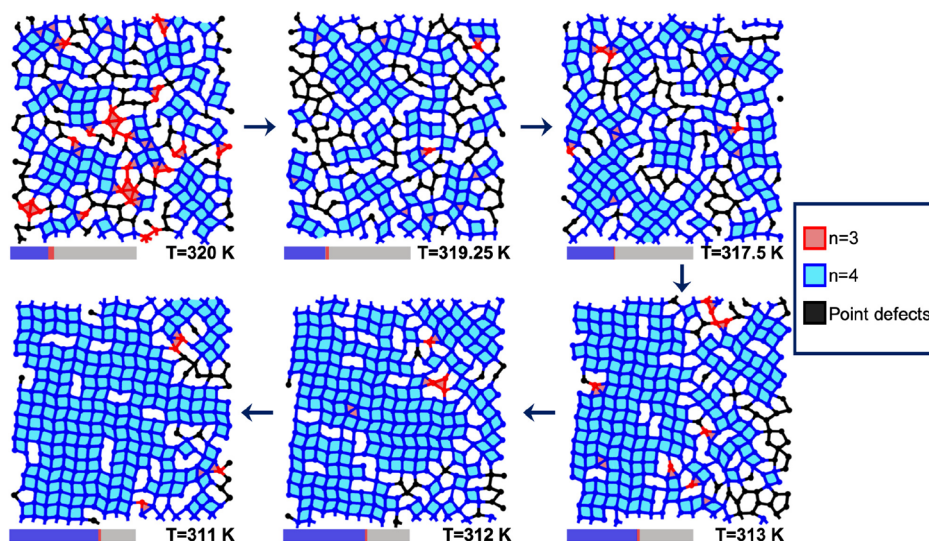


Figure 7. Snapshots of monolayer water being cooled from 320 K to 310 K at 1 GPa. The stacked bars in the lower left corner of each snapshot denote the coverage area percentages for the four-membered rings (blue) and three-membered rings (red). The colors of the particles, bonds, and interior ring shading are shown in the legend.

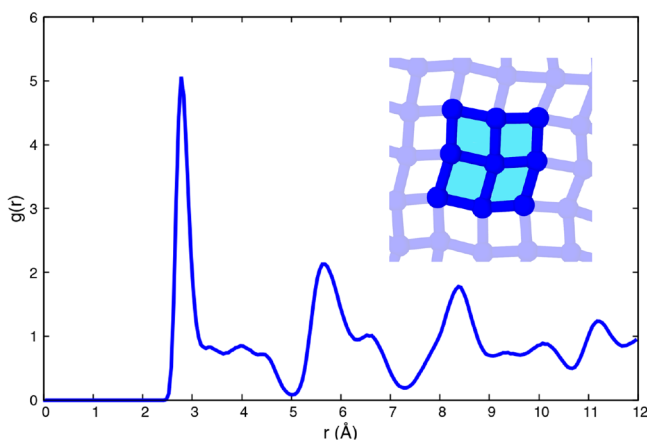


Figure 8. In-plane oxygen–oxygen radial distribution function of the ice formed at 310 K and $P_{zz} = 1$ GPa. The inset shows the four-membered rings characteristic of fMSI.

Table 1. Ring Statistics and Coverage Area Percentage for Triangular and Square Ices

| number of nodes | coverage area, a_n (%) | number of rings |
|-----------------|--------------------------|---------------------|
| $n = 4$ | 74.422 ± 3.345 | 238.94 ± 10.723 |
| $n = 3$ | 0.877 ± 0.5 | 6.2 ± 3.544 |

Figure 9b shows the (11,0) SWNT subjected to an axial pressure of $P_{zz} = 1$ MPa. Under these conditions, the INT is predominantly composed of tetragonal prism blocks, with intermittent deformed prism blocks.

The length of the INT in Figure 9a is smaller than that in Figure 9b. The number of prism blocks of each type is an unreliable indicator that does not qualitatively describe the relative proportions of the prismatic ice phases. Although a volume-based metric has been proposed,³⁶ an approximate metric based on the normalized number of prism blocks may be used as a reasonable approximation of relative proportion.

We have observed that the average height of each prism block remains relatively constant at a value of 2.845 ± 0.07 Å irrespective of the number of nodes in the basal ring, n , and

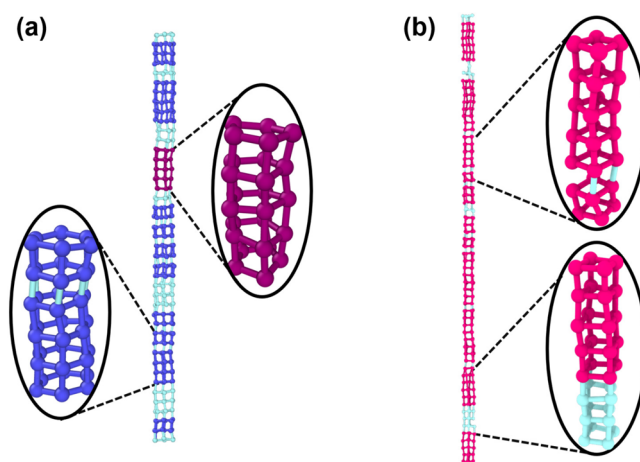


Figure 9. View of ice structures at 240 K confined within (a) a (13,0) zigzag nanotube at 0.1 MPa and (b) an (11,0) zigzag nanotube at 1 MPa. The unclassified phase, either water or deformed prism blocks, is shown in sea-green. Prism blocks of pentagonal, hexagonal, and tetragonal ices are shown in purple, blue, and pink, respectively.

even the applied pressure P_{zz} . Therefore, it is possible to define a theoretical maximum possible number of n -gonal prism blocks, assuming that the entire SWNT height is filled with n -gonal prism blocks, each of height ~ 2.845 Å. Since the average height of the prism blocks is independent of n , the theoretical maximum number of prism blocks is the same for all n . The theoretical maximum number of prism blocks, N_{\max} is thus given by

$$N_{\max} = \frac{H_{\text{SWNT}}}{h_{\text{avg}}}$$

where H_{SWNT} is the height (in Å) of the SWNT and $h_{\text{avg}} = 2.845$ Å is the average height of the prism blocks.

The normalized height percentage, H_n , for any prismatic ice phase is defined as follows:

$$H_n = \frac{N_n}{N_{\max}} \times 100$$

where N_{\max} is the theoretical maximum possible number of n -gonal prism blocks and N_n is the actual number of n -gonal prism blocks.

Table 2 summarizes the relative proportions of n -gonal prism blocks for the SWNTs. N_{\max} is the same for every n , and

Table 2. Relative Proportions of n -Gonal Prism Blocks

| SWNT type | N_n | N_{\max} | H_n (%) | V_n (%) |
|-----------|------------|------------|------------------|------------------|
| (11,0) | $N_4 = 40$ | 63 | $H_4 = 63.492\%$ | $V_4 = 69.611\%$ |
| (13,0) | $N_5 = 4$ | 43 | $H_5 = 9.302\%$ | $V_5 = 9.658\%$ |
| | $N_6 = 16$ | | $H_6 = 37.21\%$ | $V_6 = 42.982\%$ |

thus, the (11,0) and (13,0) SWNTs have $N_{\max} = 63$ and $N_{\max} = 43$, respectively, for all n . It is evident that the normalized height percentages H_n match reasonably well with the occupied volume percentages (V_n).

Freezing of an Ice Nanotube. We track the phase change from the liquid to the solid state in water confined within a (13,0) featureless nanotube, approximating a zigzag carbon nanotube. The temperature is lowered in steps of 10 K. Simulations are run in the $NP_{zz}T$ ensemble, subjected to a constant axial pressure $P_{zz} = 0.5$ MPa, for 20 ns at each temperature.

We observe an abrupt change in phase from the liquid state to the ordered prismatic ice phase at a temperature of 280 K. In the previous section, we showed how the H_n metric matches well with the occupied volume percentage, which has been proven to be an effective order parameter for nucleation of quasi-one-dimensional systems.³⁶ Thus, the phase change of an INT can be described by the H_n order parameter. Figure 10 depicts the phase change from the liquid phase, at the beginning of the simulation, to $\sim 60\%$ hexagonal prismatic phase after the 20 ns simulation time. The dominant ice phase formed is the hexagonal prismatic phase, with small proportions of pentagonal ice (within $H_5 = 7\%$). A movie in the Supporting Information documents this phase change.

CONCLUSION

d-SEAMS is a flexible postprocessing analysis tool that is capable of classifying water at both extremes of scale: highly confined systems as well as bulk water. d-SEAMS is the first scientific software to use nix as a build system to circumvent dependency clashes, along with a YAML-Lua scripting pipeline. The Lua scripting interface and the C++ API are meant to provide enough rigor for customization while still being user-friendly and accessible to the general scientific community.

Several applications of qualitative analysis have been presented. We have shown how d-SEAMS is capable of determining the time evolution of structures, from which the growth mechanism and new physical insights have been inferred for heterogeneous nucleation. A new order parameter for determining the relative composition of n -gonal ice in quasi-one-dimensional nanotubes has been formulated and implemented. The new order parameter, the height percentage H_n , produces results that match well with previously defined metrics in the literature. We have demonstrated the versatility of d-SEAMS by performing detailed structural analysis for homogeneous nucleation, fMSI formation, and ice nanotube freezing from the liquid state.

Soft matter, nanoparticle systems, and colloidal systems reportedly exhibit local order, glassy behavior, and other interesting phase transitions.^{52–57} Several of the topological network algorithms implemented in d-SEAMS make no a priori assumptions about the system and depend solely on positional data and neighbor particle cutoffs. Thus, these criteria, particularly ring statistics and prism block classification, can be applied to analyze local order and clustering phenomena in general.

d-SEAMS (<https://dseams.info>) is a free and open-source molecular dynamics analysis engine distributed on GitHub under the GNU General Public License Version 3 and documented online (<https://docs.dseams.info>). We envisage future development to incorporate more input formats and general structural analysis algorithms.⁵⁸ Given the nature of the

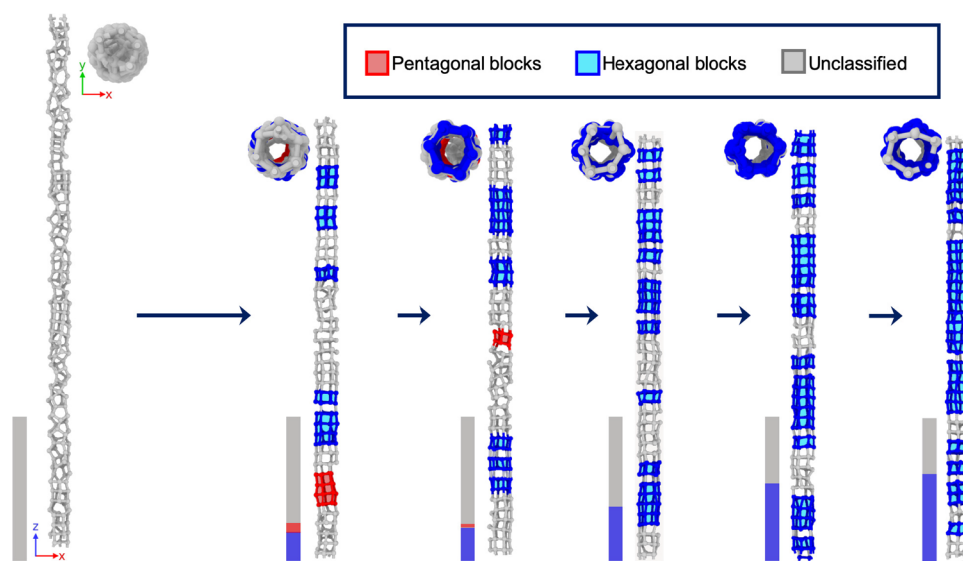


Figure 10. Snapshots of an icy nanoribbon at various time steps, at 280 K and $P_{zz} = 0.5$ MPa, in a (13,0) smooth single-walled nanotube. The stacked bars in the lower left corner of each snapshot denote the height percentages for the dominant phases: hexagonal prism blocks (blue) and pentagonal prism blocks (red). Initially, the quasi-one-dimensional water is entirely in the liquid phase.

engine, we expect additions to the framework that will provide insights into biomolecular systems as well.

■ ASSOCIATED CONTENT

Supporting Information

The Supporting Information is available free of charge at <https://pubs.acs.org/doi/10.1021/acs.jcim.0c00031>.

(PDF)

Movie showing the ordered hydrogen-bonding network in flat monolayer square ice (MPG)

Movie showing the growth of the largest ice-like cluster during homogeneous nucleation (MPG)

Movie showing the liquid-to-solid phase transition in a quasi-one-dimensional nanotube (MPG)

■ AUTHOR INFORMATION

Corresponding Author

Jayant K. Singh – Department of Chemical Engineering, Indian Institute of Technology Kanpur, Kanpur 208016, Uttar Pradesh, India; orcid.org/0000-0001-8056-2115; Phone: 0512-259 6141; Email: jayantks@iitk.ac.in; Fax: 0512-259 0104

Authors

Rohit Goswami – Department of Chemical Engineering, Indian Institute of Technology Kanpur, Kanpur 208016, Uttar Pradesh, India; orcid.org/0000-0002-2393-8056

Amrita Goswami – Department of Chemical Engineering, Indian Institute of Technology Kanpur, Kanpur 208016, Uttar Pradesh, India; orcid.org/0000-0001-8706-2383

Complete contact information is available at: <https://pubs.acs.org/doi/10.1021/acs.jcim.0c00031>

Author Contributions

[‡]R.G. and A.G. contributed equally to this work.

Notes

The authors declare no competing financial interest.

■ ACKNOWLEDGMENTS

The computational resources were provided by the HPC facility of the Computer Center (CC), Indian Institute of Technology Kanpur. R.G. acknowledges the invaluable support of his lab PI, D. Goswami.

■ REFERENCES

- (1) Stukowski, A. Structure Identification Methods for Atomistic Simulations of Crystalline Materials. *Modell. Simul. Mater. Sci. Eng.* **2012**, *20*, 045021.
- (2) Carignano, M. A. Formation of Stacking Faults during Ice Growth on Hexagonal and Cubic Substrates. *J. Phys. Chem. C* **2007**, *111*, 501–504.
- (3) Herlach, D. M.; Palberg, T.; Klassen, I.; Klein, S.; Kobold, R. Overview: Experimental Studies of Crystal Nucleation: Metals and Colloids. *J. Chem. Phys.* **2016**, *145*, 211703.
- (4) Woodcock, L. Entropy Difference between the Face-Centred Cubic and Hexagonal Close-Packed Crystal Structures. *Nature* **1997**, *385*, 141–143.
- (5) Reinhart, W. F.; Long, A. W.; Howard, M. P.; Ferguson, A. L.; Panagiotopoulos, A. Z. Machine Learning for Autonomous Crystal Structure Identification. *Soft Matter* **2017**, *13*, 4733–4745.
- (6) Lupi, L.; Hudait, A.; Molinero, V. Heterogeneous Nucleation of Ice on Carbon Surfaces. *J. Am. Chem. Soc.* **2014**, *136*, 3156–3164.

- (7) Cox, S. J.; Kathmann, S. M.; Slater, B.; Michaelides, A. Molecular Simulations of Heterogeneous Ice Nucleation. I. Controlling Ice Nucleation through Surface Hydrophilicity. *J. Chem. Phys.* **2015**, *142*, 184704.

- (8) Bi, Y.; Cao, B.; Li, T. Enhanced Heterogeneous Ice Nucleation by Special Surface Geometry. *Nat. Commun.* **2017**, *8*, 15372.

- (9) Petrenko, V.; Whitworth, R. *Physics of Ice*; Oxford University Press, 2002.

- (10) Salzmann, C. G.; Hallbrucker, A.; Finney, J. L.; Mayer, E. Raman Spectroscopic Study of Hydrogen Ordered Ice XIII and of its Reversible Phase Transition to Disordered Ice V. *Phys. Chem. Chem. Phys.* **2006**, *8*, 3088.

- (11) Salzmann, C. G.; Hallbrucker, A.; Finney, J. L.; Mayer, E. Raman Spectroscopic Features of Hydrogen-Ordering in Ice XII. *Chem. Phys. Lett.* **2006**, *429*, 469–473.

- (12) Salzmann, C. G.; Radaelli, P. G.; Mayer, E.; Finney, J. L. Ice XV: A New Thermodynamically Stable Phase of Ice. *Phys. Rev. Lett.* **2009**, *103*, 105701.

- (13) Falenty, A.; Hansen, T. C.; Kuhs, W. F. Formation and Properties of Ice XVI Obtained by Emptying a Type sII Clathrate Hydrate. *Nature* **2014**, *516*, 231–233.

- (14) del Rosso, L.; Celli, M.; Ulivi, L. New Porous Water Ice Metastable at Atmospheric Pressure Obtained by Emptying a Hydrogen-Filled Ice. *Nat. Commun.* **2016**, *7*, 13394.

- (15) Algara-Siller, G.; Lehtinen, O.; Wang, F.; Nair, R.; Kaiser, U.; Wu, H.; Geim, A.; Grigorieva, I. Square Ice in Graphene Nanocapillaries. *Nature* **2015**, *519*, 443–445.

- (16) Agrawal, K. V.; Shimizu, S.; Drahushuk, L. W.; Kilcoyne, D.; Strano, M. S. Observation of Extreme Phase Transition Temperatures of Water Confined inside Isolated Carbon Nanotubes. *Nat. Nanotechnol.* **2017**, *12*, 267–273.

- (17) Zhao, W.-H.; Bai, J.; Yuan, L.-F.; Yang, J.; Zeng, X. C. Ferroelectric Hexagonal and Rhombic Monolayer Ice Phases. *Chem. Sci.* **2014**, *5*, 1757–1764.

- (18) Takaiwa, D.; Hatano, I.; Koga, K.; Tanaka, H. Phase Diagram of Water in Carbon Nanotubes. *Proc. Natl. Acad. Sci. U. S. A.* **2008**, *105*, 39–43.

- (19) Bai, J.; Angell, C.; Zeng, X. Guest-Free Monolayer Clathrate and its Coexistence with Two-Dimensional High-Density Ice. *Proc. Natl. Acad. Sci. U. S. A.* **2010**, *107*, 5718–5722.

- (20) Salzmann, C. G.; Radaelli, P. G.; Slater, B.; Finney, J. L. The Polymorphism of Ice: Five Unresolved Questions. *Phys. Chem. Chem. Phys.* **2011**, *13*, 18468.

- (21) Salzmann, C. G. Advances in the Experimental Exploration of Water's Phase Diagram. *J. Chem. Phys.* **2019**, *150*, 060901.

- (22) Chen, J.; Schusteritsch, G.; Pickard, C. J.; Salzmann, C. G.; Michaelides, A. Two Dimensional Ice from First Principles: Structures and Phase Transitions. *Phys. Rev. Lett.* **2016**, *116*, 025501.

- (23) Koga, K.; Tanaka, H.; Zeng, X. First-Order Transition in Confined Water between High-Density Liquid and Low-Density Amorphous Phases. *Nature* **2000**, *408*, 564–567.

- (24) Zangi, R.; Mark, A. E. Monolayer Ice. *Phys. Rev. Lett.* **2003**, *91*, 025502.

- (25) Bai, J.; Zeng, X. Polymorphism and Polyamorphism in Bilayer Water Confined to Slit Nanopore under High Pressure. *Proc. Natl. Acad. Sci. U. S. A.* **2012**, *109*, 21240–21245.

- (26) Zhu, Y.; Wang, F.; Bai, J.; Zeng, X. C.; Wu, H. Compression Limit of Two-Dimensional Water Confined in Graphene Nanocapillaries. *ACS Nano* **2015**, *9*, 12197–12204.

- (27) Zhu, Y.; Wang, F.; Bai, J.; Zeng, X. C.; Wu, H. Formation of Trilayer Ices in Graphene Nanocapillaries under High Lateral Pressure. *J. Phys. Chem. C* **2016**, *120*, 8109–8115.

- (28) Gao, Z.; Giovambattista, N.; Sahin, O. Phase Diagram of Water Confined by Graphene. *Sci. Rep.* **2018**, *8*, 6228.

- (29) Boettger, C. An Introduction to Docker for Reproducible Research. *SIGOPS Oper. Syst. Rev.* **2015**, *49*, 71–79.

- (30) Dolstra, E.; de Jonge, M.; Visser, E. Nix: A Safe and Policy-Free System for Software Deployment. In *Proceedings of the 18th USENIX Conference on System Administration*; USENIX, 2004; pp 79–92.

- (31) Prins, J.; Suresh, J.; Dolstra, E. *Nix Fixes Dependency Hell on All Linux Distributions*; Linux, 2008.
- (32) Rein ten Wolde, P.; Ruiz-Montero, M. J.; Frenkel, D. Numerical Calculation of the Rate of Crystal Nucleation in a Lennard-Jones System at Moderate Undercooling. *J. Chem. Phys.* **1996**, *104*, 9932–9947.
- (33) Li, T.; Donadio, D.; Russo, G.; Galli, G. Homogeneous Ice Nucleation from Supercooled Water. *Phys. Chem. Chem. Phys.* **2011**, *13*, 19807.
- (34) Franzblau, D. Computation of Ring Statistics for Network Models of Solids. *Phys. Rev. B: Condens. Matter Mater. Phys.* **1991**, *44*, 4925–4930.
- (35) Haji-Akbari, A.; Debenedetti, P. G. Direct Calculation of Ice Homogeneous Nucleation Rate for a Molecular Model of Water. *Proc. Natl. Acad. Sci. U. S. A.* **2015**, *112*, 10582–10588.
- (36) Goswami, A.; Singh, J. K. A General Topological Network Criterion for Exploring the Structure of Icy Nanoribbons and Monolayers. *Phys. Chem. Chem. Phys.* **2020**, *22*, 3800–3808.
- (37) Steinhardt, P. J.; Nelson, D. R.; Ronchetti, M. Bond-Orientational Order in Liquids and Glasses. *Phys. Rev. B: Condens. Matter Mater. Phys.* **1983**, *28*, 784–805.
- (38) Moore, E. B.; de la Llave, E.; Welke, K.; Scherlis, D. A.; Molinero, V. Freezing, Melting and Structure of Ice in a Hydrophilic Nanopore. *Phys. Chem. Chem. Phys.* **2010**, *12*, 4124.
- (39) Nguyen, A. H.; Molinero, V. Identification of Clathrate Hydrates, Hexagonal Ice, Cubic Ice, and Liquid Water in Simulations: The CHILL+ Algorithm. *J. Phys. Chem. B* **2015**, *119*, 9369–9376.
- (40) Stukowski, A. Visualization and Analysis of Atomistic Simulation Data with OVITO—the Open Visualization Tool. *Modell. Simul. Mater. Sci. Eng.* **2010**, *18*, 015012.
- (41) Humphrey, W.; Dalke, A.; Schulten, K. VMD: Visual Molecular Dynamics. *J. Mol. Graphics* **1996**, *14*, 33–38.
- (42) Dolstra, E.; Löb, A. NixOS. *SIGPLAN Not.* **2008**, *43*, 367.
- (43) Shirts, M. R.; Klein, C.; Swails, J. M.; Yin, J.; Gilson, M. K.; Mobley, D. L.; Case, D. A.; Zhong, E. D. Lessons Learned from Comparing Molecular Dynamics Engines on the SAMPL5 Dataset. *J. Comput.-Aided Mol. Des.* **2017**, *31*, 147–161.
- (44) Stoddard, S. D. Identifying Clusters in Computer Experiments on Systems of Particles. *J. Comput. Phys.* **1978**, *27*, 291–293.
- (45) Vonnegut, B. The Nucleation of Ice Formation by Silver Iodide. *J. Appl. Phys.* **1947**, *18*, 593–595.
- (46) Zielke, S. A.; Bertram, A. K.; Patey, G. N. A Molecular Mechanism of Ice Nucleation on Model AgI Surfaces. *J. Phys. Chem. B* **2015**, *119*, 9049–9055.
- (47) Abascal, J.; Sanz, E.; García Fernández, R.; Vega, C. A Potential Model for the Study of Ices and Amorphous Water: TIP4P/Ice. *J. Chem. Phys.* **2005**, *122*, 234511.
- (48) Prerna; Goswami, R.; Metya, A. K.; Shevkunov, S.; Singh, J. K. Study of Ice Nucleation on Silver Iodide Surface with Defects. *Mol. Phys.* **2019**, *117*, 3651–3663.
- (49) Zielke, S. A.; Bertram, A. K.; Patey, G. Simulations of Ice Nucleation by Model AgI Disks and Plates. *J. Phys. Chem. B* **2016**, *120*, 2291–2299.
- (50) Molinero, V.; Moore, E. B. Water Modeled As an Intermediate Element between Carbon and Silicon†. *J. Phys. Chem. B* **2009**, *113*, 4008–4016.
- (51) Yang, L.; Guo, Y.; Diao, D. Structure and Dynamics of Water Confined in a Graphene Nanochannel under Gigapascal High Pressure: Dependence of Friction on Pressure and Confinement. *Phys. Chem. Chem. Phys.* **2017**, *19*, 14048–14054.
- (52) Earnshaw, J. C.; Harrison, M. B. J.; Robinson, D. J. Local Order in Two-Dimensional Colloidal Aggregation. *Phys. Rev. E: Stat. Phys., Plasmas, Fluids, Relat. Interdiscip. Top.* **1996**, *53*, 6155–6163.
- (53) Zykova-Timan, T.; Horbach, J.; Binder, K. Monte Carlo Simulations of the Solid-Liquid Transition in Hard Spheres and Colloid-Polymer Mixtures. *J. Chem. Phys.* **2010**, *133*, 014705.
- (54) Schoberth, H. G.; Emmerich, H.; Holzinger, M.; Dulle, M.; Förster, S.; Gruhn, T. Molecular Dynamics Study of Colloidal Quasicrystals. *Soft Matter* **2016**, *12*, 7644–7654.
- (55) Anderson, J. A.; Antonaglia, J.; Millan, J. A.; Engel, M.; Glotzer, S. C. Shape and Symmetry Determine Two-Dimensional Melting Transitions of Hard Regular Polygons. *Phys. Rev. X* **2017**, *7*, 021001.
- (56) Coslovich, D.; Ozawa, M.; Berthier, L. Local Order and Crystallization of Dense Polydisperse Hard Spheres. *J. Phys.: Condens. Matter* **2018**, *30*, 144004.
- (57) Mizuno, R.; Okumura, K.; Oguri, J.; Terao, T. Generalised Local Bond Order Parameter Analysis: Application to Colloidal Particles with Dendritic Polymer Brushes. *Mol. Simul.* **2019**, *45*, 743–751.
- (58) Tribello, G. A.; Giberti, F.; Sosso, G. C.; Salvalaglio, M.; Parrinello, M. Analyzing and Driving Cluster Formation in Atomistic Simulations. *J. Chem. Theory Comput.* **2017**, *13*, 1317–1327.